Investigation of blood rheology under steady and unidirectional large amplitude oscillatory shear

Jeffrey S. Horner[a)], Matthew J. Armstrong[b)], Norman J. Wagner[a)], and Antony N. Beris[a)*]

[a)]Center for Molecular and Engineering Thermodynamics and Department of Chemical and Biomolecular Engineering, University of Delaware, Newark, DE 19716
[b)]Department of Chemistry and Life Science, United States Military Academy, West Point, NY 10996
[*]Author to whom correspondence should be addressed; electronic mail: beris@udel.edu

Abstract

We present new dynamic rheological tests of human blood that motivate an improved model for the thixotropic shear rheology of human blood. Unidirectional large amplitude oscillatory shear (UD-LAOS) is proposed as a dynamic test relevant for understanding in vivo arterial pulsatile blood flow, and data are obtained for two healthy donors studied previously using more traditional steady and step-rate experiments. The model analyzes the overall extra stress of the system in two components. A thixotropic component is represented by a structure-kinetics model coupled with a stress expression containing both viscous and thixotropic elements to account for the presence of linear aggregates of red blood cells, known as rouleaux, which form at low shear rates. Another component is viscoelastic, described through an extend White-Metzner approach. It corresponds to the stresses that arise due to the isolated red blood cells, which deform at high shear rates. The combined model is fit to experimental steady shear and UD-LAOS data for two healthy donors and is subsequently used to predict the stress response of the blood sample to UD-LAOS experiments over a broad range of strain amplitudes and frequencies. Comparison to an earlier model for transient blood rheology shows a significantly improved fit over a range of physiologically relevant flow conditions. In addition, this analysis demonstrates the usefulness of UD-LAOS tests with regards to understanding the microstructural evolution in blood under transient flow.

I. INTRODUCTION

Thixotropy is a time-dependent rheological phenomenon that is characterized by a continual decrease in viscosity when a sample previously at rest is subjected to flow [1,2]. This phenomenon is associated with a microstructure that dynamically responds depending on the current rate of shear and stress present in the system. In general, the viscosity of a thixotropic sample recovers once flow is reduced, reflecting a time and shear dependent viscosity. Due to the vast number of materials that demonstrate thixotropy, a number of recent attempts have been made to model the time dependence of this microstructural formation and how it relates to the bulk rheological properties of the specific sample [3–5].

Blood is a particularly interesting, naturally occurring suspension that has been shown to demonstrate thixotropy as well as a variety of other interesting rheological signatures including viscoelasticity and a nonzero yield stress [6–8]. As blood is primarily a suspension of red blood cells and plasma with white blood cells and platelets accounting for relatively low volume fractions, most of these rheological phenomena may be attributed to the interactions between the suspended red blood cells. Under low shear and stasis, the red blood cells form linear aggregates [9], as shown in Fig. 1. Due to the biconcave disk shape that red blood cells commonly exhibit, these aggregates are characterized by their

unique coin stack structures known as rouleaux. These rouleaux will break apart when sheared and subsequently reform when shear is reduced giving, rise to thixotropy. Moreover, the presence of these rouleaux at low shear rates enables blood to demonstrate its nonzero yield stress and distinctive shear thinning behavior. Because various diseases have been linked to increased rouleaux formation within blood, a number of studies have been performed in an attempt to better understand this process.

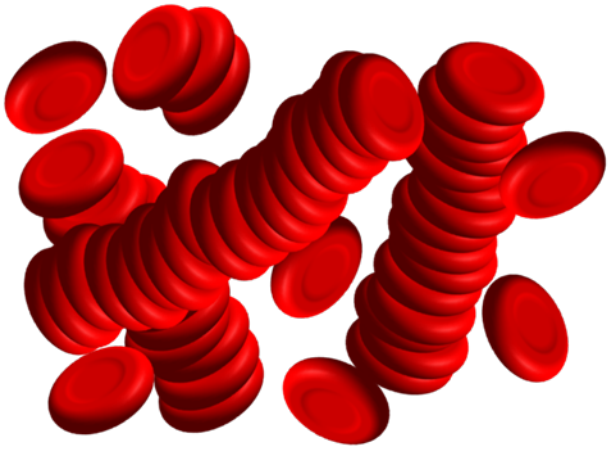

FIG. 1. Depiction of linear rouleaux that red blood cells will form at stasis and low shear rates. This image is based qualitatively on images of red blood cell rouleaux [9].

Previous studies have shown that red blood cells will aggregate in the presence of macromolecules [10]. For in vivo conditions, fibrinogen, a protein within the plasma, has been shown to most significantly affect the aggregation tendencies of red blood cells [11]. Two prevailing theories describe the mechanics of aggregation of red blood cells into rouleaux. The first theory is the "bridging" theory, which suggests that these macromolecules can adsorb onto the surface of the red blood cells. Through Brownian motion, two red blood cells will come into contact, and the macromolecules may form a bridge between the two surfaces [10,11]. This theory has been supported by in vitro experiments using dextran, which found that separation distance between red blood cells increases with dextran molecular weight [12], consistent with a longer bridge length.

Alternatively, a second theory proposes that a depletion of macromolecules exists near the red blood cell membranes due to electrostatic hindrance and configurational entropy losses. The overlap of two depletion layers of adjacent red blood cells yields a net attraction between the red blood cells through osmotic pressure [13,14]. This theory has been supported by work which has found that the aggregation tendencies of red blood cells are heavily dependent on the hydrodynamic radii of macromolecules as opposed to the specific macromolecule [15]. Moreover, unlike the bridging hypothesis, the depletion hypothesis does not require the adsorbed macromolecules to dynamically readjust to form the rouleaux structures.

Another factor contributing to the bulk rheology of blood is the finite deformability of red blood cells. At high shear rates ($>100\ s^{-1}$), blood will continue to demonstrate a shear thinning behavior, although less pronounced, which cannot be attributed to rouleaux formation as rouleaux should no longer be present under these conditions. Various authors have investigated this phenomenon through experiments and simulations and have attributed the shear thinning nature at high shear rates to the deformability of the red blood cells [16,17]. At moderate shear rates, the red blood cell motion will transition from a tumbling behavior to a tank treading behavior resulting in a decreased viscosity. Additionally, it was found that hardened red blood cells have a significantly increased bulk viscosity without shear thinning behavior at high shear rates [18,19]. In vivo, the deformability of red blood cells

is a critical component that enables transport to capillaries that may have dimensions smaller than the individual red blood cell.

The steady shear rheology of blood has been previously well explored, and various works have used differing constitutive models such as the Casson [20], Cross [21], Carreau [22], Carreau-Yasuda [23], and Quemada [24] models to represent the viscosity of blood over a range of shear rates. More recently, several works have attempted to correlate the parameters of these models to the physiological properties of the blood sample [25–27]. Far fewer attempts have been performed to model the transient behavior of human blood rheology. Several authors have used microscopic simulations of red blood cells in an attempt to predict the bulk rheological behavior of human blood [17,28]. However, these models are often computationally expensive and can only be implemented in carefully chosen flow geometries, further indicating the need for a simplified bulk rheological model. Notable attempts for bulk rheology thixotropic models of blood have been implemented using a multi-mode Maxwell approach based on polymer network theory [29], a structural based thixotropic approach that exhibits a Casson dependence under steady shear [30], and a thermodynamically stable generalized Oldroyd-B approach [31]. Although many of these approaches have shown potential in modeling blood accurately for specific flow conditions, the lack of reliable transient data on human blood rheology hinders model parametrization and validation.

As blood is a living, biological fluid, both a thorough understanding of its biology and rheology are required to obtain accurate measurements on the sample. It has been well documented that blood will change with extended time from withdrawal, including both a change in deformability of the red blood cells [32] as well as a change in aggregation of the red blood cells [33]. Moreover, storage temperature has also been shown to affect the measureable time for accurate rheology measurements on blood [34]. However, care is required for cooled samples to ensure the cells are not damaged, and ample time is required to rewarm to physiological temperature. Other experimental factors, such as interfacial effects, evaporation, and sedimentation must also be taken into account. These effects can often be mitigated by selecting an appropriate geometry [35]. However, care must be taken in selecting the materials of construction for the geometry as many metals have been shown to affect blood through adsorption of proteins [36]. Furthermore, when blood is subjected to low shear, a red blood cell depletion layer will form near the walls of the measurement device. This “syneresis” effect is initially due to excluded volume effects but will increase over time as a result of shear migration. This phenomenon is well documented in Poiseuille flow and is known as the Fahraeus Effect [37]. Additionally, this effect has also been shown to occur in Couette flow [38]. Due to these handling complications, existing data on blood rheology that fail to fully detail the measurement protocol are often unreliable and may misrepresent the bulk rheology [39].

As a variety of conditions can arise from hyperviscosity syndromes, understanding the complex rheology that blood demonstrates can be critical in disease diagnosis, treatment, and prevention [40]. By modeling blood rheology, one can obtain information about the microscopic interactions occurring within the blood sample which can potentially lead to evaluation of the physiology of a particular blood sample. Consequently, it has been proposed that blood rheology may be used as an efficient diagnostic tool for a number of these syndromes. Moreover, modeling the rheology of blood is critical for accurate construction of blood flow models throughout the circulatory system. Currently, the most sophisticated models for in vivo blood flow only account for the steady shear behavior of blood rheology often using a generalized Newtonian constitutive model [41]. However, as blood flows naturally in pulsatile conditions, it is necessary to account for the thixotropic elements of blood rheology as well. These blood flow models have potential for a wide range of applications including use in nutrient transport throughout the body as well as treatment of stenoses or other blood flow complications.

In this paper, a new thixotropic model is presented for human blood rheology which incorporates elements of the modified Delaware thixotropic model (MDTM) proposed by Armstrong *et al.* [5] coupled with a shear dependent viscoelastic term to account for the deformation of the red blood cells.

The new model is also compared to a previous model proposed by Apostolidis *et al*., henceforth referred to as the AAB model [30] (see the Supplemental Material, Section S-I for a complete formulation of the AAB model). The AAB model is a more specific version of the MDTM that had previously been used to fit blood rheology data. Upon fitting the parameters of the new model to both transient and steady shear experiments, the model is used to predict the stress response of human blood to novel unidirectional large amplitude oscillatory shear (UD-LAOS) tests over a range of frequencies and amplitudes. The results are then compared with new experimental transient data obtained on healthy human blood. The UD-LAOS tests used are imposed on the sample through a superposition of an oscillatory shear in the nonlinear regime and a steady shear equal in amplitude to the oscillation. The superposition of the steady shear prevents the flow from reversing and results in a similar flow to in vivo pulsatile conditions. We also provide a framework for understanding the stress signature of UD-LAOS experiments which can be used for future material characterization.

The remainder of the paper will proceed as follows. In Section 2, we present the model formulation by first considering the motion of free red blood cells where no structure is present. The structural contribution is then added to achieve the full model. In Section 3, we outline the experimental methodology and protocol. Additionally, the fitting protocol and methodology for evaluating the model predictions will be described with a focus on UD-LAOS. In Section 4, we show the results as well as the experimental data we have obtained on healthy human blood and provide a comparison with a previously developed thixotropic model for blood rheology. In Section 5, we provide a discussion of the model and address the present limitations. Lastly, in Section 6, we present our conclusions.

II. MODEL FORMULATION

Our constitutive model incorporates a thixotropic component representing rouleaux structure at low shear rates and a viscoelastic component representing deformation of the individual red blood cells at high shear rates. The structural component of the model involves a nondimensional structure parameter [35], λ, which represents the current level of rouleaux formation within the blood sample and ranges from 0 (no structure present) to 1 (fully structured).

A. Individual Red Blood Cells Contribution

First consider the case where no structure is present in the sample ($\lambda = 0$) and the red blood cells are all freely suspended. In this situation, no yield stress will be present in the sample as shown by previous experimental works on red blood cells suspended in an albumin-Ringer solution [16]. Despite the absence of structure formation, the free red blood cells continue to demonstrate a shear thinning behavior that is characterized by a shear dependent change from a zero viscosity ($\mu_{0,C}$) to an infinite shear viscosity ($\mu_{\infty,C}$). This steady shear behavior of the individual red blood cell shear stress contribution, $\sigma_{SS,12,C}$, is represented by a Cross model with the exponential term set to 1:

$$\sigma_{SS,12,C} = \eta_{SS,C}(\dot{\gamma})\dot{\gamma} = \left(\frac{\mu_{0,C}-\mu_{\infty,C}}{1+\tau_C|\dot{\gamma}|} + \mu_{\infty,C}\right)\dot{\gamma}\,, \tag{1}$$

where τ_C is a time constant governing the dependence of the apparent viscosity under steady shear, $\eta_{SS,C}$, on the shear rate, $\dot{\gamma}$.

In addition to demonstrating shear thinning under steady shear, a suspension of free red blood cells will also exhibit viscoelasticity, which may be seen through oscillatory tests on whole blood at high frequencies and high amplitudes. These experiments will be shown in Section 4. A number of differential constitutive models exist in literature that may be used to capture this viscoelastic element of

the red blood cell transient stress contribution, $\boldsymbol{\sigma_C}$ [42–44]. The White-Metzner model offers a relatively simple way to couple the shear dependent viscosity, η_C, with viscoelastic effects:

$$\boldsymbol{\sigma_C} + \left(\frac{\eta_C(\dot{\gamma})}{G_C}\right)\boldsymbol{\sigma_C}_{(1)} = \eta_C(\dot{\gamma})\boldsymbol{\gamma}_{(1)} \,, \tag{2}$$

where $\boldsymbol{\sigma_C}_{(1)}$ and $\boldsymbol{\gamma}_{(1)}$ are the upper convected time derivatives of the stress and deformation respectively and G_C represents the elastic modulus of the suspension of individual blood cells [45]. However, previous work has shown that the original formulation of the White-Metzner model can result in a loss of evolution and offers no way of extracting structural information from the model [46]. These potential inconsistencies and shortcomings arise due to the direct dependency of the viscosity on the shear rate. However, they can be alleviated through an extended White-Metzner model which reformulates the viscosity to be a function of the first invariant of the conformation tensor, $\boldsymbol{c}$, [46]:

$$\boldsymbol{\sigma_C} + \left(\frac{\eta_C(c_I)}{G_C}\right)\boldsymbol{\sigma_C}_{(1)} = \eta_C(c_I)\boldsymbol{\gamma}_{(1)} \tag{3}$$

$$\boldsymbol{\sigma_C} = G_C(\boldsymbol{c} - \boldsymbol{\delta}) \,, \tag{4}$$

where $\boldsymbol{\delta}$ is the unit tensor and the stress tensor, $\boldsymbol{\sigma_C}$, is assumed to be of the form:

$$\boldsymbol{\sigma_C} = \begin{pmatrix} \sigma_{11,C} & \sigma_{12,C} & 0 \\ \sigma_{12,C} & 0 & 0 \\ 0 & 0 & 0 \end{pmatrix}, \tag{5}$$

for one dimensional shear flow. Because the conformation tensor is directly linked to the stress tensor, Eq. (3) may be rewritten by reformulating the viscosity to be a function of the first invariant of the stress tensor, $\sigma_{I,C}$, and thus, only one dependent tensor quantity is present:

$$\boldsymbol{\sigma_C} + \left(\frac{\eta_C(\sigma_{I,C})}{G_C}\right)\boldsymbol{\sigma_C}_{(1)} = \eta_C\left(\sigma_{I,C}\right)\boldsymbol{\gamma}_{(1)} \,. \tag{6}$$

Using the assumption of a Cross-like steady shear behavior for the individual red blood cells, we can obtain an expression for the transient viscosity as a function of the first invariant of the stress tensor. This invariant is the trace of the stress tensor which is defined as the sum of the diagonal tensor components. For the stress tensor prescribed in Eq. (5), the first invariant and its respective steady state value are:

$$\sigma_{I,C} = \mathrm{tr}(\boldsymbol{\sigma_C}) = \sigma_{11,C} + 0 + 0 = \sigma_{11,C} \overset{SS}{\Rightarrow} \sigma_{I,SS,C} = \frac{2\eta_{SS,C}^2\dot{\gamma}^2}{G_C} \,, \tag{7}$$

such that the steady shear viscosity due to the red blood cells can be resolved (see the Supplemental Material, Section S-II) through:

$$b = \tau_C\sqrt{\frac{G_C\sigma_{I,C}}{2}} - \mu_{0,C} \tag{8}$$

$$c = -\mu_{\infty,C}\tau_C\sqrt{\frac{G_C\sigma_{I,C}}{2}} \tag{9}$$

$$\eta_C\left(\sigma_{I,C}\right) = \frac{-b-\sqrt{b^2-4c}}{2} \,. \tag{10}$$

The transient shear stress contribution from the red blood cells, $\sigma_{12,C}$, is governed by the formulation outlined in Eq. (6), i.e.:

$$\sigma_{12,C} + \left(\frac{\eta_C(\sigma_{I,C})}{G_C}\right)\frac{d\sigma_{12,C}}{dt} = \eta_C(\sigma_{I,C})\dot{\gamma} \ . \tag{11}$$

A more detailed derivation of the governing stress equation is provided in the Supplemental Material, Section S-II. This model formulation provides a thermodynamically consistent representation of the isolated red blood cell viscoelastic contributions while reducing to the Cross model under steady shear conditions.

B. Rouleaux Contribution

At low shear rates, red blood cells aggregate to form rouleaux, which significantly increase the bulk viscosity and lead to a nonzero yield stress. For the current model, the level of rouleaux formation is represented by a nondimensional structure parameter, λ, which grows according to a differential rate equation containing a Brownian aggregation term, a shear induced aggregation term, and a shear breakup term:

$$\frac{d\lambda}{dt} = \frac{1}{\tau_\lambda}\left((1-\lambda) + (1-\lambda)\tau_a\left|\dot{\gamma}_p\right| - \lambda\left(\tau_b\dot{\gamma}_p\right)^2\right), \tag{12}$$

where τ_λ is a time constant governing the overall rate of structure formation and breakdown, τ_a is a time constant governing the relative rate of structure formation due to shearing, and τ_b is a time constant governing the relative rate of shear induced structure breakdown. Note that in this equation, the structure parameter is constrained to vary between 1, indicating a fully structured sample at zero shear, and 0, indicating no structure present, which occurs at infinite shear. The specific shear stress contribution of the rouleaux is the sum of elastic and viscous components:

$$\sigma_R = \lambda G_R\gamma_e + \lambda^3\mu_R\dot{\gamma}_p \ , \tag{13}$$

where G_R is the elastic modulus for the rouleaux, μ_R is the model viscosity for the rouleaux, and γ_e and $\dot{\gamma}_p$ are the red blood cell elastic strain and plastic rate of shear respectively. Based on low Reynolds number hydrodynamics, the viscous stress contribution is proportional to λ^3 due to the assumption that the structure parameter is linked to the average length of the rouleaux [35]. Consequently, through this identification, the viscosity is a function of the effective hydrodynamic volume occupied by the rouleaux. In contrast, the elastic stress exhibits a linear dependence on the structure parameter, λ, as this stress arises from a network contribution, and the simplest dependence on the structure parameter was selected ensuring that these elastic stresses disappear in the absence of structure.

The modulus of the rouleaux, G_R, is related to the structure parameter by a simple differential relaxation equation:

$$\frac{dG_R}{dt} = \frac{1}{\tau_G}\left(\frac{G_{0,R}}{\lambda} - G_R\right), \tag{14}$$

where τ_G is a time constant governing the rate of relaxation for the elastic modulus arising from the roueaux. The steady state value for the elastic modulus arising from rouleaux is inversely proportional to the structure parameter. This arises do to the assumption that the structure parameter is in some way

linked to the average length of the rouleaux, and for linear springs in series, the equivalent elastic modulus is inversely proportional to the length. It should be noted that the elastic modulus is not bounded in this expression. This is reflective of a strain stiffening system, and due to the later specification of the maximum allowable elastic strain, will not be an issue as the structure parameter approaches zero. Alternatively, an upper bound for the elastic modulus could be prescribed. However, this value would need to be large to not limit the system and could not be accurately determined from the measurements. The fully structured elastic modulus, $G_{0,R}$, is defined as:

$$G_{0,R} = \frac{\sigma_y}{\gamma_{0,R}}, \tag{15}$$

where σ_y represents the yield stress and $\gamma_{0,R}$ represents the maximum elastic strain. Note that these parameters can, in principle be obtained by an independent strain sweep. The elastic strain imposed on the rouleaux is calculated by using an adaptation of the kinematic hardening model previously described by Apostolidis *et al.* [4,30], which begins by decomposing the total strain and rate of strain into an elastic and plastic component as:

$$\gamma = \gamma_e + \gamma_p \leftrightarrow \dot{\gamma} = \dot{\gamma}_e + \dot{\gamma}_p \, . \tag{16}$$

It should be noted that Eq. (16) neglects the changes in elastic strain that arise from structural breakdown. The elastic strain rate is given by:

$$\dot{\gamma}_e = \begin{cases} \dot{\gamma}_p - \frac{\gamma_e}{\gamma_{max}}\left|\dot{\gamma}_p\right|, & \frac{d\gamma_{max}}{dt} \geq 0 \\ \dot{\gamma}_p - \frac{\gamma_e}{\gamma_{max}}\left|\dot{\gamma}_p\right| + \frac{\gamma_e}{\gamma_{max}}\frac{d\gamma_{max}}{dt}, & \frac{d\gamma_{max}}{dt} < 0 \end{cases}, \tag{17}$$

in which the maximum elastic strain sustained by the rouleaux, γ_{max}, is defined as:

$$\gamma_{max} = \gamma_{0,R}\lambda \, . \tag{18}$$

This formulation for the elastic rate of strain is modified slightly from the AAB model to account for the changes in the maximum elastic strain due to structure breakup. As the structure is destroyed, the current level of elastic strain should be constrained to be less than or equal to the maximum sustainable elastic strain. Note that this derivative may be solved for explicitly by differentiating Eq. (18) and using the expression for the rate of change of the structure parameter, Eq. (12). The formulation for the maximum elastic strain, Eq. (18), was chosen to reflect the shrinking size of the rouleaux as structure is destroyed. The specific plastic component of the rate of strain on the rouleaux can be evaluated by neglecting structure breakup effects and combining Eq. (16) and Eq. (17) to yield:

$$\dot{\gamma}_p = \begin{cases} \frac{\dot{\gamma}}{\left(2-\frac{\gamma_e}{\gamma_{max}}\right)}, & \dot{\gamma} \geq 0 \\ \frac{\dot{\gamma}}{\left(2+\frac{\gamma_e}{\gamma_{max}}\right)}, & \dot{\gamma} < 0 \end{cases}. \tag{19}$$

The overall shear stress exhibited by the blood sample, σ_{Tot}, is a combination of the stress from the rouleaux, σ_R, and that from the red blood cells, $\sigma_{12,C}$. This is achieved through a direct summation of the two contributing stress components:

$$\sigma_{Tot} = \sigma_{12,C} + \sigma_R \ , \tag{20}$$

where the red blood cell stress component is found from Eq. (11), and the rouleaux stress component is found from Eq. (13). It should be noted that while the model is able to predict the full tensorial stress for the red blood cell contribution, the stress contribution from the rouleaux is limited to only the shear stress at this time. This is a consequence of using a scalar order parameter to describe the rouleaux structure.

C. Steady Shear Solution

Under steady shear conditions, any deformation occurring will occur plastically as:

$$\dot{\gamma}_{p,SS} = \dot{\gamma} \ , \tag{21}$$

and the elastic strain will reach its previously defined maximum value:

$$\gamma_{e,SS} = \gamma_{R0}\lambda_{SS}^2 \ . \tag{22}$$

In addition, the time derivative in the rate equation for the structural parameter, Eq. (12), is set to zero, enabling one to obtain a solution for the structural parameter as a function of the steady shear rate:

$$\lambda_{SS} = \frac{1+\tau_a|\dot{\gamma}|}{1+\tau_a|\dot{\gamma}|+(\tau_b\dot{\gamma})^2} \ , \tag{23}$$

and the elastic modulus of the rouleaux has fully relaxed to its equilibrium value, given by:

$$G_{R,SS} = \frac{G_{0,R}}{\lambda_{SS}} \ . \tag{24}$$

Substituting Eqs. (21)-(24) into Eq. (13) and utilizing the relation in Eq. (15) gives the rouleaux stress contribution under steady shear:

$$\sigma_{SS,R} = \sigma_y \left(\frac{1+\tau_a|\dot{\gamma}|}{1+\tau_a|\dot{\gamma}|+(\tau_b\dot{\gamma})^2}\right) + \mu_R\dot{\gamma}\left(\frac{1+\tau_a|\dot{\gamma}|}{1+\tau_a|\dot{\gamma}|+(\tau_b\dot{\gamma})^2}\right)^3 \ . \tag{25}$$

Finally, to obtain the total stress exhibited by the blood sample under steady shear, σ_{SS}, the steady shear rouleaux stress contribution, $\sigma_{SS,R}$, must be added to the steady shear red blood cell contribution as given by Eq. (1):

$$\sigma_{Tot,SS} = \left(\frac{\mu_0-\mu_\infty}{1+\tau_C|\dot{\gamma}|} + \mu_\infty\right)\dot{\gamma} + \sigma_y \left(\frac{1+\tau_a|\dot{\gamma}|}{1+\tau_a|\dot{\gamma}|+(\tau_b\dot{\gamma})^2}\right) + \mu_R\dot{\gamma}\left(\frac{1+\tau_a|\dot{\gamma}|}{1+\tau_a|\dot{\gamma}|+(\tau_b\dot{\gamma})^2}\right)^3 \ . \tag{26}$$

Upon examination of Eq. (26) one can observe that at high shear rates, the rouleaux contribution will go to zero and the blood will exhibit Cross-like behavior until finally reaching a purely Newtonian behavior with a viscosity of μ_∞. As the shear rate goes to zero, the rouleaux contribution will dominate the red blood cell contribution and eventually, the total stress will approach the yield stress, σ_y.

III. METHODS

A. Sampling and Measurement Protocol

The sampling and measurement protocols are the topic of a separate forthcoming publication, and only the key aspects will be presented here. All experimental results presented in this work were obtained from two healthy human blood samples, and these procedures were implemented in compliance with UD's Institutional Review Board. Samples were collected by a licensed nurse practitioner at the Nurse Managed Primary Care Center located at the University of Delaware STAR campus. Both donors sampled were not currently taking any medication and had no known health complications. Prior to withdrawal, both donors had undergone fasting for 8 to 10 hours. Upon withdrawal, both donors were placed in a seated position and a tourniquet was applied. The blood was drawn from the antecubital vein using a 21 G needle and was collected into a 6 mL Vacutainer tube containing 1.8 mg/mL of ethylenediaminetetraacetic acid (EDTA) as an anticoagulant. This procedure is in compliance with guidelines established by the International Society of Clinical Hemorheology [47]. Additionally, three separate tubes of blood were obtained from each donor and sent to Quest Diagnostics for Complete Blood Count, Lipid Panel, and Fibrinogen Activity testing. Results of these tests are summarized in Table I.

TABLE I. Physiological properties of the two blood samples which the model was fit to.

Property	Units	Donor 1	Donor 2
Hematocrit	%	42.6	40.8
Fibrinogen	mg/dL	186	287
Total Cholesterol	mg/dL	126	205
Triglycerides	mg/dL	51	94
HDL Cholesterol	mg/dL	48	71
LDL Cholesterol	mg/dL	68	115

Measurements on all blood samples were performed in an ARES-G2 strain control rheometer from TA Instruments equipped with a double wall Couette geometry. This rheometer can measure shear rates over a wide range and has a minimum torque and angular frequency of 0.1 μN.m and 1 μrad/s respectively. The geometry was selected to maximize contact surfaces and the vertical orientation while minimizing interfacial area and required loading volume. The bob is composed of titanium and the cup stainless steel, materials that have been shown to have insignificant interactions with blood [36]. For the inner wall, the measurement gap is 0.43 mm, and the measurement gap for the outer wall is 0.5 mm. The required loading volume for this geometry is 5 mL.

Both blood samples were measured at 37.0 °C. This temperature was maintained using a Peltier temperature controller with a sensitivity of 0.1 °C. To minimize effects of aging, all measurements were completed within 4 hours of withdrawal. Prior to measuring the samples, the blood underwent a transportation period of 45 to 60 minutes during which the sample was stored at room temperature. The sample was loaded into the measurement geometry using a 5 mL syringe equipped with a 21 G needle. A solvent trap was used to minimize effects of evaporation, and the sample was allowed 5 minutes to equilibrate to the temperature before testing. To prevent damage to the red blood cells, shear rates within the rheometer never exceeded 1000 s^{-1}. A preshear of 300 s^{-1} for 30 s was implemented between subsequent tests to remove any memory effects from the previous test.

B. Rheological Tests Conducted

In this work, experimental data are presented for steady and dynamic measurements performed on the blood samples. The first test conducted on the sample upon loading into the rheometer and temperature equilibration was a steady shear curve at shear rates ranging from 0.1 s^{-1} to 700 s^{-1}. For each shear rate, the sample was measured for 40 s or a minimum strain of 50. For shear rates above 2 s^{-1}, the steady shear stress value was taken as the average of the final 15 transient stress measurements obtained on the sample. As for shear rates at or below 2 s^{-1}, the steady shear stress response was taken as the maximum of the transient data. This method is in compliance with previously established guidelines for performing steady shear measurements on human blood and is implemented to account for the effects of syneresis, which can result in significantly lower measured stresses particularly at low shear rates.

In addition to the steady shear measurements, unidirectional large amplitude oscillatory shear (UD-LAOS) tests were also performed which are similar in theory and interpretation to standard large amplitude oscillatory shear (LAOS) experiments. UD-LAOS experiments were previously introduced to study thixotropic suspensions [5]. These novel tests involve a superposition of a standard LAOS experiment with a steady shear equal in amplitude to the oscillatory shear imposed:

$$\dot{\gamma}(t) = \gamma_0 \omega \cos(\omega t) + \gamma_0 \omega \ . \tag{27}$$

These UD-LAOS measurements are implemented on the sample to best match the in vivo pulsatile flow conditions typical in arterial flows. All UD-LAOS tests presented were carried out until a steady behavior, i.e., alternance, was observed. The evolution to this final steady profile is not shown.

Similar to LAOS, for UD-LAOS tests, the dynamic stress response may be interpreted as a function of the transient oscillatory strain and shear rate defined by:

$$\gamma_t(t) = \gamma_0 \sin(\omega t) \ , \tag{28}$$
$$\dot{\gamma}_t(t) = \gamma_0 \omega \cos(\omega t) \ , \tag{29}$$

respectively [5]. In these coordinates, the transient oscillatory stress is not zero on average during the cycle. Using these variables, elastic and viscous projections of the UD-LAOS stress response, i.e., Lissajous-Bowditch plots, can be constructed in a manner similar to LAOS. For reference, the expected qualitative elastic and viscous projections for various model fluids is presented in Fig. 2. In these relative coordinates, the shape of a cycle for a linearly viscoelastic fluid and a Newtonian fluid to a UD-LAOS experiment will be identical to the corresponding shape for a LAOS experiment. On the other hand, a simple Casson fluid [20],

$$\sqrt{\sigma} = \sqrt{\sigma_y} + \sqrt{\mu \dot{\gamma}} \ , \tag{30}$$

will show a qualitatively different behavior in UD-LAOS, as shown in Fig. 2. Thus, UD-LAOS tests provide a means to independently vary the frequency and amplitude of a dynamic test while eliminating the effects of microstructure reorientation associated with flow reversals.

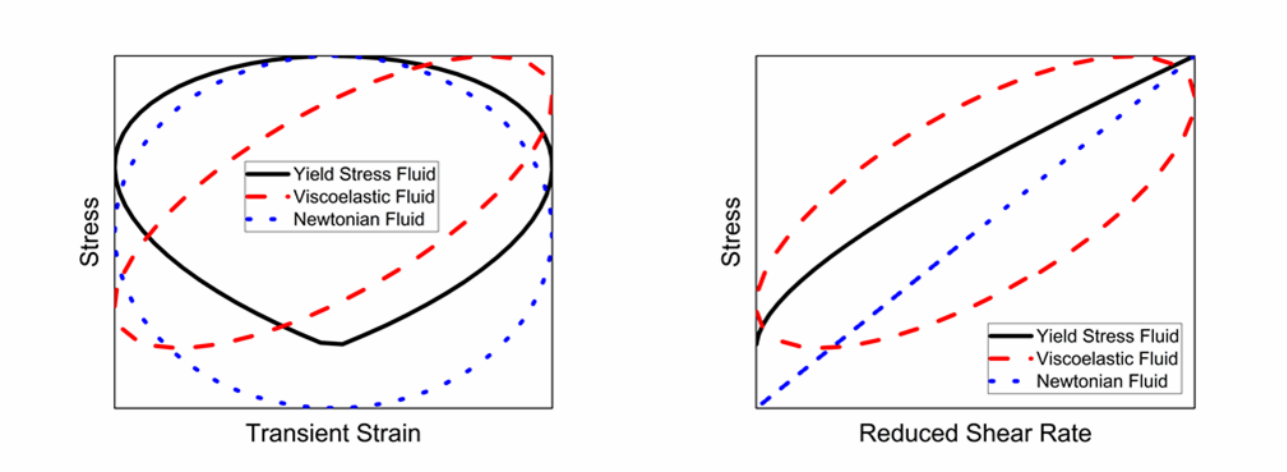

FIG. 2. Qualitative (a) elastic and (b) viscous projections of expected stress signatures to a UD-LAOS experiment for model fluids: Casson fluid (solid), Maxwell fluid (dashed), Newtonian fluid (dotted).

C. Model Fitting Procedure

In total, 11 parameters in the model must be fit to experimental data. Seven of these parameters may be fit to the steady shear data, where three govern the red blood cell deformability at high shear rates ($\mu_{0,C}$, $\mu_{\infty,C}$, and τ_C) and four govern the rouleaux formation at low shear rates (σ_y, τ_a, τ_b, and μ_R). These parameters are detailed in Table II. However, through an analysis of the steady shear data available, it was observed that the shear aggregation dominates the Brownian aggregation term over all measured shear rates. Thus, a constant value of 10 s was assumed for the time constant for structure breakdown, τ_b, and the low shear parameters may effectively be reduced to a set of three parameters (σ_y, τ_b^2/τ_a , and μ_R). This value for the structure breakdown time constant was selected as the inverse of the lowest measured steady shear rate to ensure that the shear dependent terms dominated the Brownian term over all measured shear rates. The exact value for this parameter would need to be determined through a flow cessation experiment. To account for the effects of aging in the sample over time from withdrawal, the set of steady shear parameters were determined from two flow curve measurements obtained at the beginning and end of testing. As the values vary slightly with time, the steady shear parameter values used were determined by taking the stress weighted average of the steady shear parameter values fit to each test, using the preshear for each UD-LAOS test as the relative weighting. To not bias the structural breakdown time constant, the time constant for shear induced aggregation, τ_a, was also assumed to be constant. The value used for this parameter was taken as the average of the values determined at the beginning and end of the experiments.

The remaining four parameters (G_C, $G_{0,R}$, τ_λ, and $\gamma_{0,R}$), detailed in Table III, were fit to several UD-LAOS experiments simultaneously at varying frequencies and amplitudes (ω=10 rad/s, γ_0=10; ω=10 rad/s, γ_0=1; ω=0.2 rad/s, γ_0=100; and ω=1 rad/s, γ_0=5), as discussed below. Because the model parameters were fit to the UD-LAOS curves after alternance had been reached, the zero shear rate limiting elastic strain for the rouleaux, $\gamma_{0,R}$, did not significantly affect the fit. Thus, this parameter was assumed to have a unitary value to be consistent with previous works [5,30]. As previously mentioned, this parameter may be resolved independently through a strain sweep experiment. The transient parameters were assumed to be constant over the measurement time.

TABLE II. Optimal steady shear model parameters for flow curve measurements taken on blood from each donor at both the beginning and end of experiments.

Parameter	Units	Description	Donor 1 Beginning	Donor 1 End	Donor 2 Beginning	Donor 2 End
$\mu_{0,C}$	mPa.s	Zero shear viscosity of suspended RBCs	7.82	7.44	8.56	10.3
$\mu_{\infty,C}$	mPa.s	Infinite shear viscosity of suspended RBCs	3.07	3.23	3.50	4.02
τ_C	s	RBC deformation coefficient	0.0383	0.0316	0.0361	0.0376
σ_y	mPa	Yield stress	1.61	2.30	1.23	3.17
τ_b	s	Time constant for structure breakdown	10	10	10	10
τ_a	s	Time constant for shear induced structure aggregation	483	561	385	411
μ_R	mPa.s	Structural viscosity contribution	9.22	9.94	30.9	41.0

TABLE III. Optimal transient model parameters for UD-LAOS measurements taken on blood from each donor.

Parameter	Units	Description	Donor 1	Donor 2
G_C	Pa	RBC elastic modulus	0.448 ± 0.008	0.639 ± 0.015
τ_λ	s	Overall structural rebuild time constant	1960 ± 20	1600 ± 20
τ_G	s	Rouleaux elastic modulus relaxation time constant	1.66 ± 0.03	1.71 ± 0.07
$\gamma_{0,R}$	--	Rouleaux zero shear rate limiting elastic strain	1	1

The parameters were fit using a multi-parameter global optimization method based on a parallel tempering algorithm proposed by Armstrong *et al*. [48]. The objective function was specified as the sum of the L_2 norms for each data set used in the fitting:

$$F_{obj} = \frac{1}{N}\sum_{k=1}^{N}\frac{1}{P_k}\frac{\|\sigma_{model}-\sigma_{data}\|_{2,k}}{\overline{\sigma}_{data,k}} . \tag{31}$$

For each of the data sets, the L_2 norm is divided by the number of points in the data set, P_k, and the average of the experimental stress data. To enable accurate comparison of objective values, the entire summation is also divided by the number of data sets, N.

The error for the experimental data was assumed to be equal to the machine's stress measurement minimum, which for the geometry used in the experiments corresponds to 0.6335 mPa. Since the objective function is a direct result of the stress residuals, and the stress error remains constant for all shear rates, no weighting of the residuals is necessary. The errors associated with the parameter estimation as shown in Table III, were determined through 10 successive executions of the model fitting methodology with pseudorandom initial guesses for the parameters. The parameter values yielding the overall lowest residuals are reported in Tables II and III. Note that for the steady shear parameters, the errors are not included as they are small relative to the optimal values (see the Supplemental Material, Section S-III). The optimal solutions for each of the 10 successive runs may be found in the Supplemental Material, Section S-III.

For comparison, a previous model for blood rheology described by Apostolidis *et al.*, which the current model contains elements of, is also fit to the experimental data [30]. Notably, the AAB model, which contains in total six parameters, differs in that it contains a different maximum elastic strain formulation, no term to account for the red blood cell deformability at high shear rates, and an

assumption of Casson behavior, Eq. (30), at low to moderate steady shear rates. For the specific formulation of this model, the reader is referred to the Supplemental Material, Section S-I. This model was fit to the same experimental data according to the previous procedure outlined by Apostolidis *et al* [30]. The optimal parameters are listed in Table IV. Note that no error bars are provided as the range of values for the optimal parameters of the AAB model was wide indicating a number of local minima and a weak dependence of the objective value on the parameters.

TABLE IV. Optimal AAB model parameters for UD-LAOS measurements taken on blood from each donor.

Parameter	Units	Description	Donor 1	Donor 2
μ	mPa.s	Casson model viscosity	3.11	3.00
σ_y	mPa	Casson yield stress	2.20	3.21
k_λ	--	Structural rate constant	8.09	9.39
k_G	--	Elastic modulus rate constant	31.9	18.3
γ_0	--	Zero shear rate limiting elastic strain	0.00439	0.00233
γ_∞	--	Infinite shear limiting elastic strain	1	1

IV. RESULTS

The data from and model fits to the initial steady shear experiments conducted on blood from both donors are shown in Fig. 3(a). The value of the structure parameter over this range is shown in the Supplemental Material, Section S-IV. These experiments were used to evaluate the six parameters previously outlined which govern the steady shear behavior of the sample. From Fig. 3(a), it is evident that the model is able to properly capture the steady shear behavior of the samples over a range of shear rates. Additionally, the current model improves upon the AAB model by accounting for observed deviations from Casson behavior, which can be seen in the Casson plots shown in Fig. 3(b). However, the steady state solution to the model contains a large number of parameters and the accuracy of the model cannot be fully assessed without transient data.

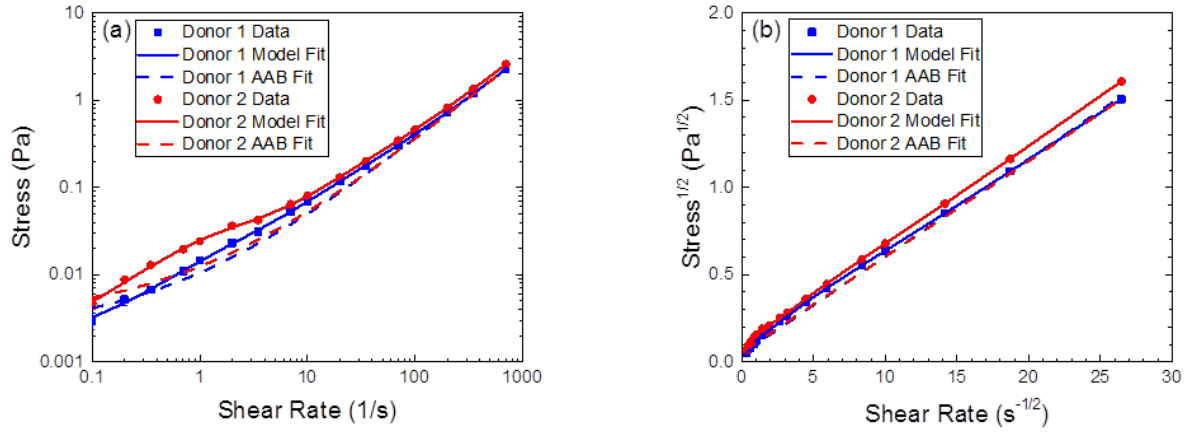

FIG. 3. The initial steady shear data (symbols) taken on blood from both donors (a) in standard coordinates and (b) Casson coordinates. Comparison of the new model fit (solid lines) with the AAB model (dashed lines) shows an improved fit which is specifically able to account for deviations from the Casson model at low shear rates.

To fit the transient parameters, four separate UD-LAOS experiments were used at conditions bracketing physiological flows. In order (a)-(d), these tests move from high frequency, high amplitude; to lower amplitude; to lower frequency, higher amplitude; and finally, moderate frequency, moderate amplitude. The elastic projections of these fits for both donors over the same times as the experimental data can be seen in Figs. 4 and 5. The viscous projections are shown in the Supplemental Material, Section S-IV. It should be noted that the time constants governing the elastic modulus relaxation for the rouleaux in both the new model and the AAB model were constrained to ensure alternance was reached over a similar time scale to the experimental data. Comparing to the model responses presented in Fig. 2 shows these blood samples exhibit primarily thixotropic behavior, as especially evident in the top-bottom asymmetry, for tests shown in Figs. 4(c) and 4(d) and with some viscoelasticity present as evident in the left-right asymmetry, most evident for the test shown in Fig. 4(a). The new model is able to capture the transient behavior exhibited by these UD-LAOS tests very well across the range of frequencies, in contrast to the AAB model. The best model fits slightly underpredict the stress for Fig. 4(b). However, the deviations are relatively small and the qualitative behavior is still captured well.

The data and model fits for Donor 2 shown in Fig. 5 demonstrate qualitatively similar behavior to that of Donor 1. However, subtle differences between the data sets exist due to the unique physiological profiles that characterize each blood sample as documented in Table I. Notably, at high frequencies and low strain amplitudes, the sample from Donor 2 stores more elastic stress which is slightly underpredicted by the model as seen in Fig. 4(b). Additionally, for moderate frequencies, the transient structure adjustment is shifted somewhat for Donor 2 as seen through a comparison between Figs. 4(d) and 5(d). For reference, the plots of the structure parameter during these UD-LAOS tests are shown in the Supplemental Material, Section S-IV for both samples as a function of the transient strain and transient shear rate. The deviations between the two data sets present an interesting opportunity to relate the bulk rheology of the samples to the physiology. Understanding this connection could unlock the potential of using rheology as a quick and inexpensive tool to identify the physiological conditions of a blood sample.

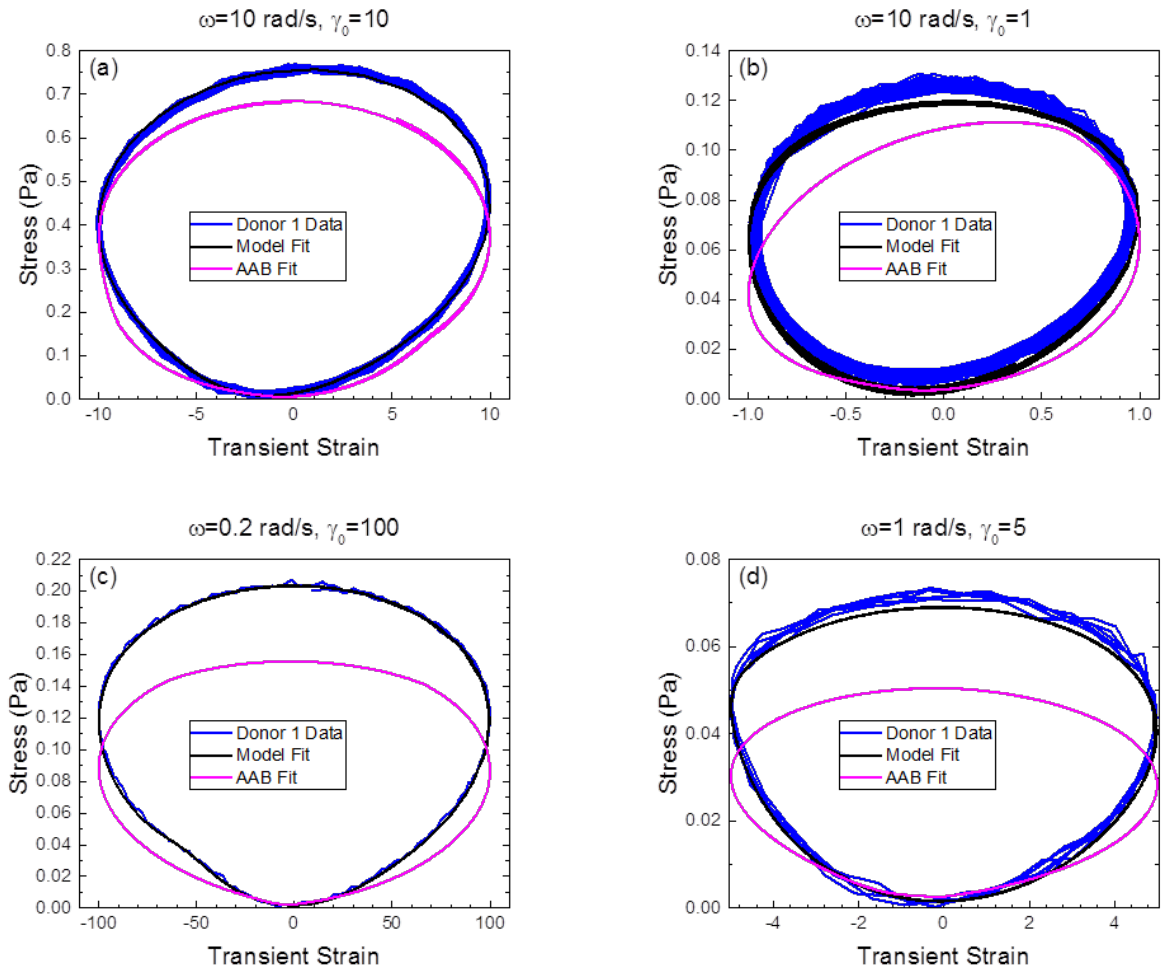

FIG. 4. Elastic projection (current and AAB) model fits to UD-LAOS experimental data on blood from Donor 1 at (a) a frequency of 10 rad/s and a strain amplitude of 10, (b) a frequency of 10 rad/s and a strain amplitude of 1, (c) a frequency of 0.2 rad/s and a strain amplitude of 100, and (d) a frequency of 1 rad/s and a strain amplitude of 5. Inspection shows that the new model provides a significantly improved fit to the data.

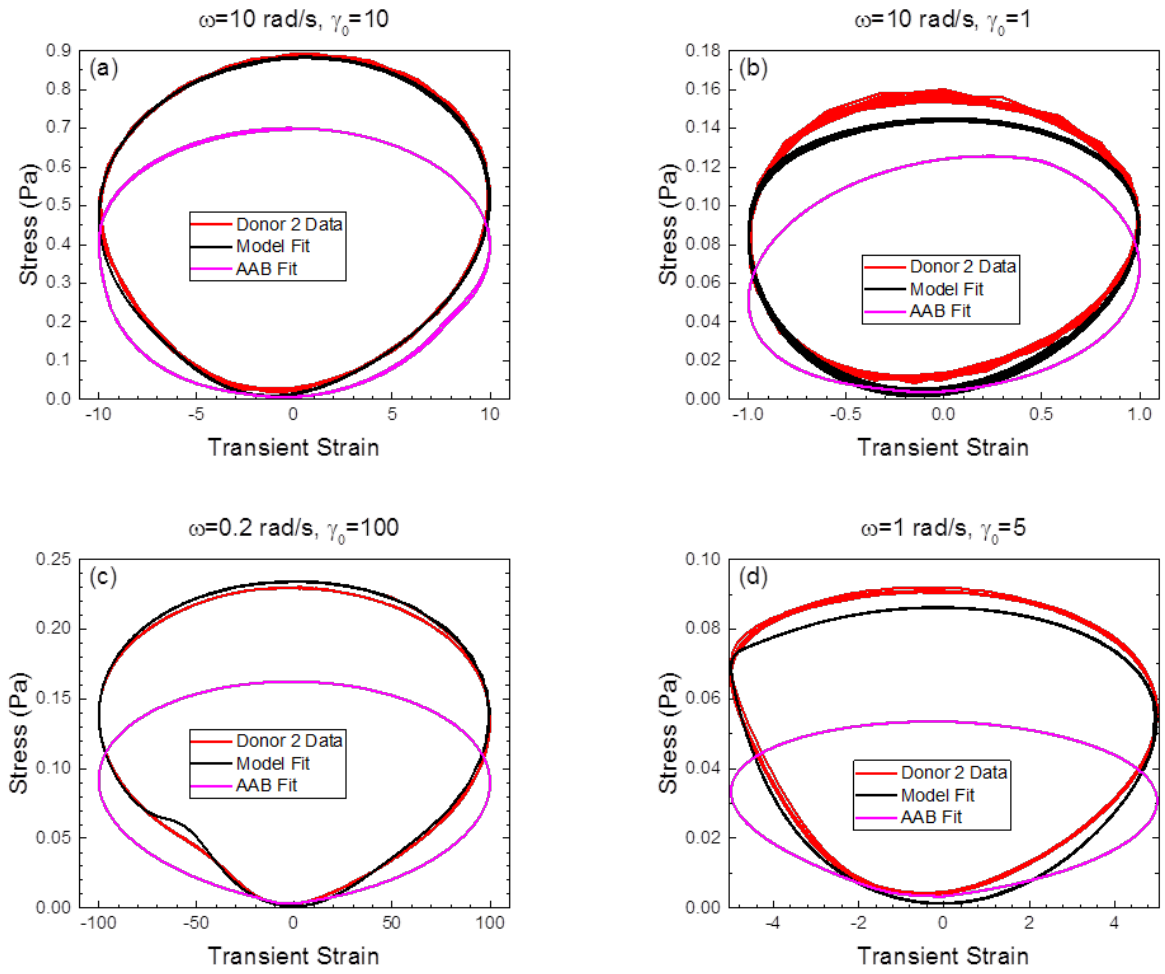

FIG. 5. Elastic projection (current and AAB) model fits to UD-LAOS experimental data on blood from Donor 2 at (a) a frequency of 10 rad/s and a strain amplitude of 10, (b) a frequency of 10 rad/s and a strain amplitude of 1, (c) a frequency of 0.2 rad/s and a strain amplitude of 100, and (d) a frequency of 1 rad/s and a strain amplitude of 5. Inspection shows that the new model provides a significantly improved fit to the data.

Using the parameters determined by the fits in Fig. 5, the stress response to additional UD-LAOS experiments may be predicted as seen by the Pipkin diagram for the Donor 2 UD-LAOS elastic projections shown in Fig. 6. The corresponding Pipkin diagram for the viscous projections is provided in the Supplemental Material, Section S-IV. Note that although not shown here, the Donor 1 data and predictions were qualitatively similar to the Donor 2 data and predictions shown in Fig. 6.

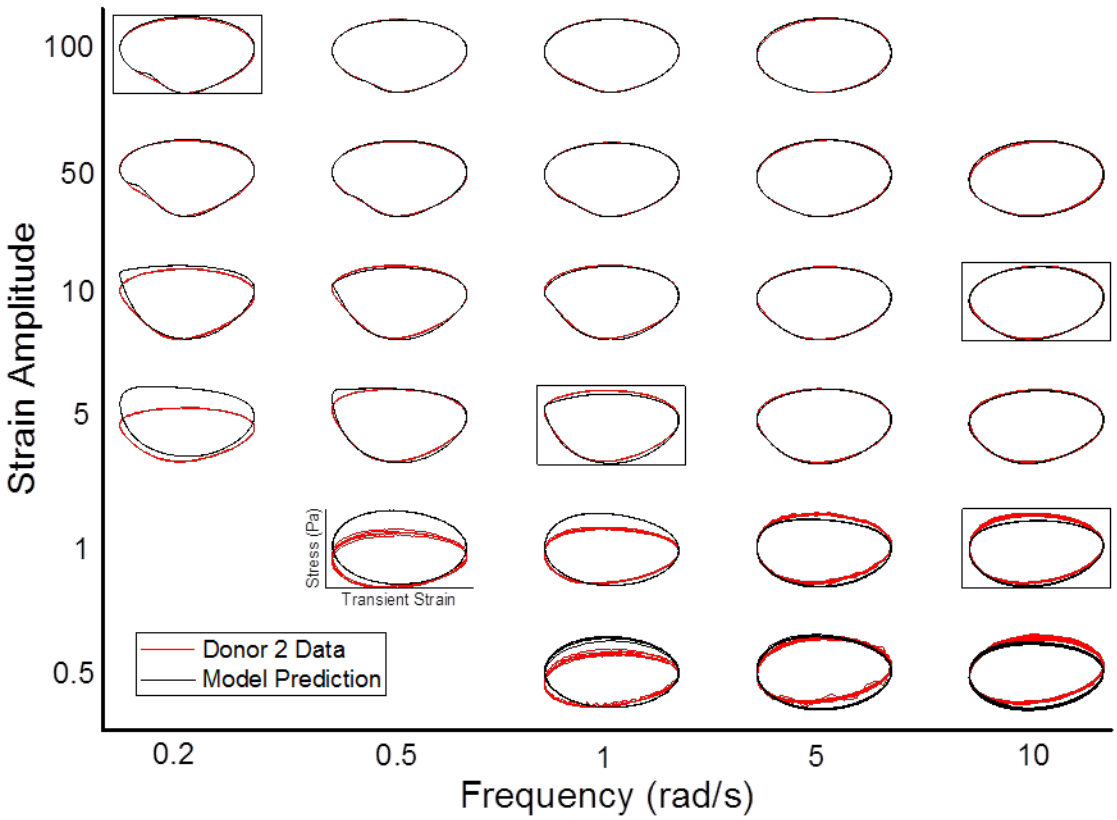

FIG. 6. Pipkin diagram of UD-LAOS elastic projections for blood from Donor 2. The model predictions are also shown with the four curves used to fit the parameters boxed. The new model is able to accurately predict the stress response of the sample over a range of conditions but deviates some at low frequencies and amplitudes. Note that the steady background shear rate during the test is equivalent to the frequency times the strain amplitude.

From the diagram in Fig. 6, different behaviors exhibited by the sample may be seen depending on the amplitude and frequency of the specific test. At large amplitudes and frequencies, the shear rates present in the system are also large and will break down any structure present. Furthermore, due to the high frequency, the structure will not have time to reform. Thus, a viscoelastic behavior will arise as seen by the left-right asymmetry which is due to the deformation of the red blood cells. As the strain amplitude is increased further, the thixotropic effects will eventually disappear.

At lower amplitudes, the shear rates present in the system will reduce. Depending on the level of reduction, rouleaux in the sample may form. The formation of these rouleaux is indicated by a fundamentally different elastic response which features a longer relaxation time than the elastic response of the deforming red blood cells. This enables the system to store additional elastic stress at high frequencies which is seen by the vertically shifted curves in the bottom right region of Fig. 6. However, the model currently underpredicts this stored stress. This is due to the fact that the elastic stress arising from the rouleaux in the model may not surpass the yield stress at maximum strain and elastic modulus equilibrium conditions.

If the frequency is decreased, the elastic response and transient structure reformation of the rouleaux may be better seen. However, if the frequency is decreased too far, the structure will have enough time to breakdown and reform which will prevent the elastic response from being observed. Instead, a response that is expected of a viscous yield stress fluid, which may be defined according to the steady shear response of the model, Eq. (26), will be observed. The model provides a good prediction to the experimental data at low frequencies and high amplitudes. However, at lower amplitudes, the model

overpredicts the stress of the sample. This is likely due to the fact that syneresis is likely to occur in this region and the model does not presently account for inhomogeneities in the sample. Syneresis will be more pronounced at these low shear rates due to the increased aggregate size and will result in a decreased stress response of the sample over long time periods.

V. DISCUSSION

The model proposed in this work improves significantly upon the original AAB model as shown through the comparison presented in Figs. 4 and 5. The AAB model fails to capture the distinct features of the UD-LAOS curves as well as the deviations from Casson behavior seen in the steady shear data. The current model fixes these shortcomings through the inclusion of a viscoelastic description of the isolated red blood cells and a reformulation of the structural contributions. Unlike the AAB model, the structural term includes both a viscous and elastic contribution to the bulk stress. The inclusion of the additional viscous structure component was realized through an analysis of the steady shear data shown in Fig. 7. In Fig. 7, the purely structural stress component, σ_R as given in Eq. (20), is shown for steady shear flow of blood from both donors. In both cases, the stress response features a peak as opposed to a monotonic decrease, which can only be described through the inclusion of additional viscous contributions associated with the presence of rouleaux.

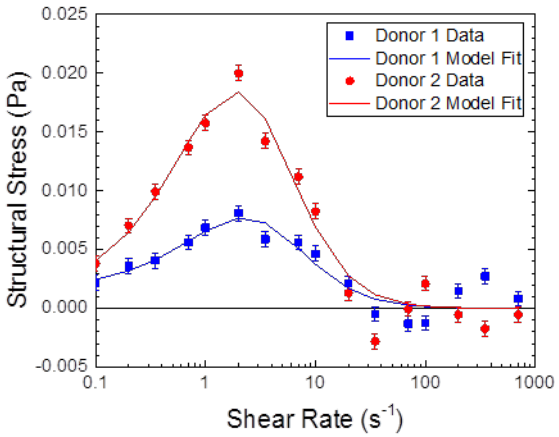

FIG. 7. Structure component of the bulk stress (solid lines: model fit; symbols: data) for two different donors at varying steady shear rates. The data demonstrate an initial increase in stress followed by a decline to zero at high shear rates signifying the need for a viscous contribution to the structural stress component.

The necessity for an additional viscoelastic component associated with the deformation of the individual red blood cells can be validated through the UD-LAOS data at 10 rad/s and a strain amplitude of 10 shown in Figs. 4(a) and 5(a). At this shear rate and frequency, the structure present in the system is destroyed and will not have time to reform. However, the data continue to demonstrate both a slight shear thinning and viscoelastic behavior. Furthermore, previous data taken by Chien on red blood cells in albumin-Ringer solution, shown in Fig. 8, demonstrate a shear thinning behavior despite the fact that no aggregation should occur within this medium [16]. The Cross model was chosen to represent this behavior due to both its simplicity and the suitability of the fit to the data shown in Fig. 8.

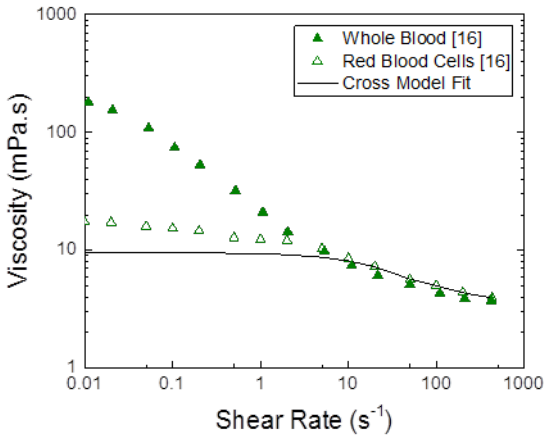

Fig. 8. Data (symbols) obtained by Chien [16] on both whole blood and red blood cells suspended in albumin-Ringer solution. The Cross model fit (solid line) is provided for the resuspended red blood cell data. Note that no error bars were provided. However, the error at low shear rates is expected to be significant.

Despite the initial success in fitting and predicting UD-LAOS tests over a range of frequencies and amplitudes, a number of areas require further investigation. From the predictions shown in Fig. 6, it is evident that there are some inconsistencies between the model predictions and the experimental data at low shear conditions. One known shortcoming of the model particularly at low shear rates is the inability to account for flow inhomogeneities, such as syneresis, which arise initially due to excluded volume effects and become more pronounced with time. This effect is significant at shear rates below 2 s^{-1} [47] and should thus affect the UD-LAOS data at the lowest frequencies and amplitudes. Although the inclusion of this effect may resolve some of the discrepancies, it is also likely that the functional dependence of the elastic contribution of the rouleaux on the structure parameter may need to be reevaluated to better capture the low shear elastic effects which likely account for the discrepancies between the data and the model fits present in Figs. 4(b) and 5(b).

There are also limitations in fitting the model parameters. Particularly, the effects of aging complicate transient data comparison. These effects were minimized by conducting the experiments in a short amount of time. However, the stress response of the sample to different tests continuously changed as a function of time from withdrawal resulting in varying parameters. Further analysis needs to be conducted on how the parameters change as a function of time from withdrawal. Additionally, despite the usefulness of the UD-LAOS tests in interpreting transient structure reformation and viscoelastic effects, these tests alone are not enough to determine all of the model parameters accurately. Particularly, we were unable to easily decouple the shear aggregation and shear breakup time constants, τ_a and τ_b respectively, due to the domination of the shear aggregation term over the Brownian aggregation term at all measured shear rates. Nevertheless, the Brownian aggregation term is critical for the full model to enable structural rebuild when no shear is present in the system. The exact contribution of this term relative to the other terms in the structural evolution equation can only be assessed through tests at very low shear rates or through flow cessation tests. The zero shear rate limiting elastic strain of the rouleaux also may not be determined from the UD-LAOS alternance data alone and requires an independent strain sweep measurement.

Lastly, the current formulation of the model is only applicable for certain flow conditions. Currently, the model is formulated only to handle unidirectional shear and may need to be adjusted to better account for flow reversals. This will be investigated in a future work. Moreover, although the viscoelastic red blood cell contribution to the stress is formulated as a full thermodynamically consistent tensor model, the structural stress component is only applicable for one dimensional shear flow. Thus, the model could in theory predict the normal stresses associated with flow in the absence of rouleaux but

has no way of predicting the response of the blood when microstructure is present. A multidimensional model of the rouleaux stress is critical both for three dimensional flow simulations in complex geometries and proper modeling of the syneresis process exhibited by blood at low shear rates.

VI. CONCLUSIONS

A new model is proposed to represent the macroscopic shear rheology of healthy human blood. The model consists of two stress components. The first stress component corresponds to the viscoelastic component of the isolated red blood cells which may deform at high shear rates. This term reduces to a Cross behavior under steady shear and utilizes an extended White-Metzner model for the transient formulation. The second stress component is associated with the formation of rouleaux within the blood and consists of both a viscous and an elastic contribution. Those stresses depend on a structure parameter, λ, which varies from 0 to 1 and evolves in time according to a kinetic rate equation. The parameters of the model are determined by fitting to both the steady shear data and four UD-LAOS curves at varying amplitudes and frequencies. Furthermore, we show that model predictions compare favorably to UD-LAOS curves measured over an extended range of amplitudes and frequencies.

Through the analysis of the model fits and predictions, the usefulness of UD-LAOS experiments are also highlighted. In the particular case of measuring blood rheology, understanding this flow type is of critical importance due to its similarity to pulsatile flow that occurs naturally in vivo at shear rates similar to ones measured in this work. However, UD-LAOS tests can be used to characterize a wide range of materials. By reformulating the strain as a transient strain, the data can be analyzed in a comparable method to standard LAOS data and provide insight into the relative thixotropic and viscoelastic effects present in the system. This also enables the experimenter to decouple the structural breakdown effects present in LAOS flow from the flow reversal effects by eliminating the backward flow component. Thus, once the structural reformation process is properly modeled for UD-LAOS flow, the effects of flow reversal can be discerned as the difference between the LAOS data and the current model prediction for LAOS flow.

The model formulated in this work significantly outperforms the AAB model which, despite previous work that showed a good fit to hysteresis ramp experiments, is unable to properly capture the stress response to UD-LAOS experiments. The AAB model fails due to the inability to deviate from Casson behavior for steady shear and the single elastic component which is unable to represent both the rouleaux and the red blood cell viscoelastic contributions. The current model is shown to be able to accurately capture a range of UD-LAOS curves, but some quantitative deviations are evident at very low shear rates. These observed deviations can be attributed to the failure to account for flow inhomogeneities and an inaccurate functional dependence of the elastic rouleaux contribution on the structural parameter.

In addition to significantly improving the fit to rheological shear data on human blood, this model can have several other impacts. Particularly, the red blood cell viscoelastic element of the model is formulated as a full tensorial model, which in theory could be used in macroscopic simulations of blood flow through arteries in which the presence of rouleaux should not dictate the flow behavior. These simulations have applications ranging from drug delivery to treatment of stenoses. Additionally, the model improves the understanding of the kinetics of rouleaux formation and the mechanical response of red blood cells to external stimuli. Since the formation of rouleaux and changes in red blood cell morphology have been linked to a variety of diseases, there is potential in correlating the rheology to the physiology of the sample and using rheology as a diagnostics tool for early signs of disease. However, a major limitation at this time is how to best evaluate the model parameters. This will be a topic of future investigation and could prove critical in unlocking the link between the bulk flow behavior of blood and the physiology.

ACKNOWLEDGMENTS

The authors would like to thank the National Science Foundation for funding through award number CBET 1510837. We would also like to acknowledge the Nurse Managed Primary Care Center at the University of Delaware STAR campus for support in drawing the blood samples, Quest Diagnostics for performing the lab tests, and the Environmental Health & Safety department at the University of Delaware for their assistance in transporting the samples. Finally, we also thank Dr. Donna S. Woulfe for her assistance with collection and her expertise with the biological interactions within blood as well as Dominic Gallo for aiding the computational analysis of the model fits.

NOMENCLATURE

$\boldsymbol{c}$	Red blood cell conformation tensor
F_{obj}	Objective function
G	Elastic modulus
k	Nondimensional rate constant
N	Number of data sets used in fitting
P	Number of points in each data set
t	Time
γ	Strain
$\boldsymbol{\gamma}$	Deformation tensor
$\dot{\gamma}$	Shear rate
$\boldsymbol{\delta}$	Unit tensor
η	Apparent viscosity
λ	Structure parameter
μ	Model viscosity
σ	Stress component
$\boldsymbol{\sigma}$	Stress tensor
τ	Time constant
ω	Oscillation frequency

SUBSCRIPTS

a	Constant governing the rate of shear induced structure formation
b	Constant governing the rate of shear induced structure breakdown
C	Red blood cell contribution
e	Elastic component
G	Constant governing the rate of relaxation for the elastic modulus
I	First invariant
p	Plastic component
R	Rouleaux contribution
SS	Steady shear
t	Transient oscillatory
Tot	Total blood shear stress
y	Yield stress
λ	Overall structure rebuild constant
0	Zero shear value or maximum strain when defining UD-LAOS
11	First normal tensor component

$_{12}$ First-second shear tensor component
$_{(1)}$ Convected time derivative
$_{\infty}$ Infinite shear value

References

[1] Mewis, J., and N. J. Wagner, "Thixotropy," Adv. Colloid Interface Sci. **147-148**, 214-227 (2009).

[2] Ewoldt, R. H., G. H. McKinley, "Mapping thixo-elasto-visco-plastic behavior," Rheol. Acta **56**, 195-210 (2017).

[3] Dullaert, K., and J. Mewis, "A structural kinetics model for thixotropy," J. Non-Newtonian Fluid Mech. **139**, 21-30 (2006).

[4] Dimitriou, C. J., R. H. Ewoldt, and G. H. McKinley, "Describing and prescribing the constitutive response of yield stress fluids using large amplitude oscillatory shear stress (LAOStress)," J. Rheol. **57**, 27-70 (2013).

[5] Armstrong, M. J., A. N. Beris, S. A. Rogers, and N. J. Wagner, "Dynamic shear rheology of a thixotropic suspension: Comparison of an improved structure-based model with large amplitude oscillatory shear experiments," J. Rheol. **60**, 433-450 (2016).

[6] Dintenfass, L., "Thixotropy of blood and proneness to thrombus formation," Circ. Res. **11**, 233-239 (1962).

[7] Thurston, G. B., "Viscoelasticity of human blood," Biophys. J. **12**, 1205-1217 (1972).

[8] Merrill, E. W., E. R. Gilliland, G. Cokelet, H. Shin, A. Britten, and R. E. Wells, "Rheology of human blood, near and at zero flow," Biophys. J. **3**, 199-213 (1963).

[9] Baskurt, O., B. Neu, and H. J. Meiselman, Red Blood Cell Aggregation (CRC Press, Boca Raton, FL, 2012).

[10] Brooks, D. E., "The effect of neutral polymers on the electrokinetic potential of cells and other charged particles III. Experimental studies on the dextran/erythrocyte system," J. Colloid Interface Sci. **43**, 700-713 (1973).

[11] Merrill E. W., E. R. Gilliland, T. S. Lee, and E. W. Salzman, “Blood rheology: Effect of fibrinogen deduced by addition,” Circ. Res. **18**, 437-446 (1966).

[12] Chien S., and K. Jan, “Ultrastructural basis of the mechanism of rouleaux formation,” Microvasc. Res. **5**, 155-166 (1973).

[13] Asakura S., and F. Oosawa, “On interaction between two bodies immersed in a solution of macromolecules,” J. Chem. Phys. **22**, 1255-1256 (1954).

[14] Baumler, H., B. Neu, E. Donath, and H. Kiesewetter, “Basic phenomena of red blood cell rouleaux formation,” Biorheology **36**, 439-442 (1999).

[15] Armstrong J. K., R. B. Wenby, H. J. Meiselman, and T. C. Fisher, “The hydrodynamic radii of macromolecules and their effect on red blood cell aggregation,” Biophys. J. **87**, 4259-4270 (2004).

[16] Chien, S., “Biophysical behavior of red cells in suspensions,” The Red Blood Cell (Academic Press, New York, 1975) Vol. 2, 1031-1133.

[17] Fedosov, D. A., W. Pan, B. Caswell, G. Gompper, and G. E. Karniadakis, “Predicting human blood viscosity in silico,” Proc. Natl. Acad. Sci. U. S. A. **108**, 11772-11777 (2011).

[18] Chien, S., S. Usami, R. J. Dellenback, and M. I. Gregersen, “Shear-dependent deformation of erythrocytes in rheology of human blood,” Am. J. Physiol. **219**, 136-142 (1970).

[19] Schmid-Schonbein, H., R. Wells, and J. Goldstone, “Influence of deformability of human red cells upon blood viscosity,” Circ. Res. **15**, 131-143 (1969).

[20] Casson, N., “A flow equation for pigment-oil suspensions of the printing ink type,” Rheology of Disperse Systems (Pergamon Press, New York, 1959) 84-104.

[21] Cross, M. M., “Rheology of non-Newtonian fluids: A new flow equation for pseudoplastic systems,” J. Colloid Sci. **20**, 417-437 (1965).

[22] Carreau, P. J., “Rheological equations from molecular network theories,” Trans. Soc. Rheol. **16**, 99-127 (1972).

[23] Yasuda, K., “Investigation of the analogies between viscometric and linear viscoelastic properties of polystyrene fluids,” (1979).

[24] Quemada, D., “A rheological model for studying the hematocrit dependence of red cell-red cell and red cell-protein interactions in blood,” Biorheology **18**, 501-516 (1981).

[25] Apostolidis, A. J., and A. N. Beris, “Modeling of the blood rheology in steady-state shear flows,” J. Rheol. **58**, 607-633 (2014).

[26] Moreno, L., F. Calderas, G. Sanchez-Olivares, L. Medina-Torres, A. Sanchez-Solis, and O. Manero, “Effect of cholesterol and triglycerides levels on the rheological behavior of human blood,” Korea-Aust. Rheol. J. **27**, 1-10 (2015).

[27] Apostolidis, A. J., and A. N. Beris, “The effect of cholesterol and triglycerides on the steady state shear rheology of blood,” Rheol. Acta **55**, 497-509 (2016).

[28] Liu, Y., and W. K. Liu, “Rheology of red blood cell aggregation by computer simulation,” J. Comput. Phys. **220**, 139-154 (2006).

[29] Owens, R. G., “A new microstructure-based constitutive model for human blood,” J. Non-Newtonian Fluid Mech. **140**, 57-70 (2006).

[30] Apostolidis, A. J., M. J. Armstrong, and A. N. Beris, “Modeling of human blood rheology in transient shear flows,” J. Rheol. **59**, 275-298 (2015).

[31] Anand, M., and K. R. Rajagopal, “A shear-thinning viscoelastic fluid model for describing the flow of blood,” Int. J. Cardiovasc. Med. Sci. **4**, 59-68 (2004).

[32] Ho, J., W. J. Sibbald, and I. H. Chin-Yee, “Effects of storage on efficacy of red cell transfusion: When is it not safe?,” Crit. Care Med. **31**, 5687-5697 (2003).

[33] Hovav, T., S. Yedgar, N. Manny, and G. Barshtein, “Alteration of red cell aggregability and shape during blood storage,” Transfusion **39**, 277-281 (1999).

[34] Uyuklu, M., M. Cengiz, P. Ulker, T. Hever, J. Tripette, P. Connes, N. Nemeth, H. J. Meiselman, and O. K. Baskurt, "Effects of storage duration and temperature of human blood on red cell deformability and aggregation," Clin. Hemorheol. Microcirc. **41**, 269-278 (2009).

[35] Mewis, J., and N. J. Wagner, Colloidal Suspension Rheology (Cambridge University Press, Cambridge, 2012).

[36] Williams, D. F., I. N. Askill, and R. Smith, "Protein adsorption and desorption phenomena on clean metal surfaces," J. Biomed. Mater. Res. **19**, 313-320 (1985).

[37] Fahraeus, R., "The suspension stability of the blood," Physiol. Rev. **9**, 241-274 (1929).

[38] Cokelet, G. R., J. R. Brown, S. L. Codd, and J. D. Seymour, "Magnetic resonance microscopy determined velocity and hematocrit distributions in a Couette viscometer," Biorheology **42**, 385-399 (2005).

[39] Sousa, P. C., J. Carneiro, R. Vaz, A. Cerejo, F. T. Pinho, M. A. Alves, and M. S. N. Oliveira, "Shear viscosity and nonlinear behavior of whole blood under large amplitude oscillatory shear," Biorheology **50**, 269-282 (2013).

[40] Kwaan, H. C., and A. Bongu, "The hyperviscosity syndromes," Semin. Thromb. Hemost. **29**, 199-208 (1999).

[41] Apostolidis, A. J., A. P. Moyer, and A. N. Beris, "Non-Newtonian effects in simulations of coronary arterial blood flow," J. Non-Newtonian Fluid Mech. **233**, 155-165 (2016).

[42] Oldroyd, J. G., "On the formulation of rheological equations of state," Proc. Royal Soc. A **200**, 523-541 (1950).

[43] Phan-Thien, N., and R. I. Tanner, "A new constitutive equation derived from network theory," J. Non-Newtonian Fluid Mech. **2**, 353-365 (1977).

[44] Giesekus, H., "A simple constitutive equation for polymer fluids based on the concept of deformation-dependent tensorial mobility," J. Non-Newtonian Fluid Mech. **11**, 69-109 (1982).

[45] White, J. L., and A. B. Metzner, “Development of constitutive equations for polymeric melts and solutions,” J. Appl. Polym. Sci. **7**, 1867-1889 (1963).

[46] Souvaliotis, A., and A. N. Beris, “An extended White-Metzner viscoelastic fluid model based on an internal structure parameter,” J. Rheol. **36**, 241-271 (1992).

[47] Baskurt, O. K., M. Boynard, G. C. Cokelet, P. Connes, B. M. Cooke, S. Forconi, F. Liao, M. R. Hardeman, F. Jung, H. J. Meiselman, G. Nash, N. Nemeth, B. Neu, B. Sandhagen, S. Shin, G. Thurston, and J. L. Wautier, “New guidelines for hemorheological laboratory techniques,” Clin. Hemorheol. Microcirc. **42**, 72-97 (2009).

[48] Armstrong, M. J., A. N. Beris, and N. J. Wagner, “An adaptive parallel tempering method for the dynamic data-driven parameter estimation of nonlinear models,” AIChE J. **63**, 1937-1958 (2016).